J. Fluid Mech. (2007), *vol.* 575, *pp.* 449–471.
doi:10.1017/S0022112006004290 Printed in the United Kingdom

Asymptotic theory of inertial convection in a rotating cylinder

KEKE ZHANG[1], XINHAO LIAO[2] AND F. H. BUSSE[3]

[1]Department of Mathematical Sciences, University of Exeter, EX4 4QE, UK
[2]Shanghai Astronomical Observatory, Chinese Academy of Sciences, Shanghai 200030, China
[3]Institute of Physics, University of Bayreuth, D-95440 Bayreuth, Germany

(Received 28 September 2005 and in revised form 11 October 2006)

Inertial convection in a fluid contained in a rotating cylinder heated uniformly from below is investigated on the basis of the assumption that convection at leading order can be represented by a single or several inertial wave modes which propagate either in the prograde or retrograde direction. Buoyancy forces appear at the next order to drive inertial convection against the effect of viscous damping. Asymptotic expressions for inertial convection for four different combinations of the sidewall boundary condition are derived for a cylinder of arbitrary aspect ratio. New convection patterns in rotating cylinders are revealed by the asymptotic analysis. A fully numerical solution of the same problem is also carried out, demonstrating a quantitative agreement between the asymptotic and numerical analysis.

1. Introduction

Through both experimental and theoretical studies, considerable progress has been made in the understanding of convective motions in a fluid-filled cylinder of depth d uniformly heated from below and rotating about its vertical axis with angular velocity Ω. Different convection modes have been identified in rotating cylinders. On the one hand, there are bulk modes which fully occupy the interior of the cylinder and which are modified forms of convection found in the non-rotating case (see, for example, Zhong, Ecke & Steinberg 1991; Goldstein *et al.* 1993). For small Prandtl numbers, Goldstein *et al.* (1994) showed numerically that there exists an exceedingly complicated behaviour at the onset of convection, including the multiplicity of convection modes at a given azimuthal wavenumber. On the other hand, wall-attached convection is found at sufficient high rates of rotation in which case the convective motions are concentrated in the vicinity of the sidewall (Zhong *et al.* 1991; Goldstein *et al.* 1993; Liu & Ecke 1999). In more detailed experimental studies, the coefficients of the Ginzburg–Landau envelope equation describing the weakly nonlinear wall-localized convection have been determined through measurements (Liu & Ecke 1999) and through theoretical studies (see, for example, Plaut 2003). It is important to note, however, that the wall-localized convection represents a boundary-layer phenomenon and, hence, cylindrical geometry plays an insignificant role (Davies-Jones & Gilman 1971; Herrmann & Busse 1993; Kuo & Cross 1993; Liao, Zhang & Chang 2005).

The present paper is concerned with convection in a rapidly rotating cylinder for which the Ekman number $E = \nu/(\Omega d^2)$, where ν is kinematic viscosity of the fluid, is sufficiently small, i.e. $E \ll 1$. It is found that there exist two fundamentally different types of convection: (i) inertial convection is preferred for fluids with small

or moderately small Prandtl numbers and (ii) wall-localized convection is preferred for fluids with intermediate or large Prandtl numbers. Inertial convection refers to fluid motions approximately represented by a single or several inertial wave modes and energetically driven by thermal buoyancy against the effect of viscous dissipation (see, for example, Zhang 1994; Busse & Simitev 2004). It is closely associated with non-axisymmetric inertial waves in a rapidly rotating cylinder. Only at low rotation rates could axisymmetric convection possibly be realized. Inertial waves describe oscillatory motions in a contained rigidly rotating homogeneous fluid which are influenced weakly by viscous dissipation occurring in the boundary layers adjacent to the bounding surfaces of the container as well as in its interior (see, for example, Greenspan 1968; Kerswell & Barenghi 1995).

The study in this paper focuses on inertial convection in rapidly rotating cylinders filled with fluids of small or moderately small Prandtl number. We derive the first asymptotic solution of inertial convection in a rotating cylinder of arbitrary aspect ratio for various combinations of thermal and velocity conditions on the sidewall. We also undertake a fully numerical analysis of the problem, showing a satisfactory quantitative agreement between the asymptotic expressions and the numerical solutions. The result of the study provides a natural bridge between two usually disjoint problems in rotating fluids: thermal convection and inertial oscillation. It also reinforces the idea that a key ingredient in the dynamics of rotating convection is the intricate interplay between the constraint of rotation and inertial and viscous effects.

It is important to recognize that there exist at least two fundamental differences between inertial convection in cylindrical and spherical geometries. In spherical geometry, the quasi-geostrophic inertial mode (Zhang *et al.* 2001) has a radial component and is directly relevant to inertial convection. The geostrophic mode in cylindrical geometry, however, does not possess a vertical component and is thus irrelevant to convective instabilities. It follows that the inertial wave modes that have the smallest frequencies are relevant to the fluid motions of inertial convection in spherical geometry (Zhang & Liao 2004), while the opposite is true for inertial convection in cylindrical geometry: the inertial wave modes with the largest frequencies are usually related to inertial convection in cylindrical geometry. More intriguingly, Zhang *et al.* (2001) showed that in spherical geometry,

$$\int_V \boldsymbol{u}^* \cdot \nabla^2 \boldsymbol{u} \, \mathrm{d}V \equiv 0, \tag{1.1}$$

where $\boldsymbol{u}$ is the velocity of any three-dimensional inertial wave, $\boldsymbol{u}^*$ is its complex conjugate and V denotes the volume of the fluid domain. This property of the vanishing integral has been used in the asymptotic analysis of inertial convection in spherical geometry (Zhang 1994). In cylindrical geometry, however, it can be shown that

$$\int_V \boldsymbol{u}^* \cdot \nabla^2 \boldsymbol{u} \, \mathrm{d}V = -\left(\frac{n\pi}{d\sigma}\right)^2 \int_V |\boldsymbol{u}|^2 \, \mathrm{d}V < 0, \tag{1.2}$$

where σ denotes the half-frequency of a three-dimensional inertial wave and $n \geqslant 1$ with $(n-1)$ denoting the number of zeros of the vertical velocity as a function of the height of the cylindrical layer. Property (1.2) offers an advantage in the derivation of asymptotic solutions for inertial convection in the cylindrical geometry.

In what follows we shall begin by presenting the mathematical equations of the problem in § 2. The numerical analysis of the problem is discussed in § 3 and asymptotic

solutions for inertial convection are derived and presented in § 4. The paper closes in § 5 with a summary and a few remarks.

2. Mathematical formulation

We consider a Boussinesq fluid in a cylinder of radius s_o with constant thermal diffusivity κ, thermal expansion coefficient α and kinematic viscosity ν. The cylinder is rotating uniformly about its axis with a constant vertical angular velocity Ω in the presence of a constant gravitational field

$$\boldsymbol{g} = -g\hat{\boldsymbol{z}}, \tag{2.1}$$

and is heated uniformly from below to produce an unstable vertical temperature gradient,

$$\nabla T_0 = -\beta\hat{\boldsymbol{z}}, \tag{2.2}$$

where β is a positive constant and cylindrical coordinates (s, ϕ, z), with the corresponding unit vectors $(\hat{\boldsymbol{s}}, \hat{\boldsymbol{\phi}}, \hat{\boldsymbol{z}})$ and $\hat{\boldsymbol{z}}$ parallel to the axis of rotation, are used. Making use of the depth of the layer d as the length scale, Ω^{-1} as the unit of time and $\beta d^3\Omega/\kappa$ as the unit of temperature fluctuations of the system, the problem of linear convective instability is governed by the equations

$$\mathrm{i}2\sigma\boldsymbol{u} + 2\hat{\boldsymbol{z}} \times \boldsymbol{u} = -\nabla p + R\Theta\hat{\boldsymbol{z}} + E\nabla^2\boldsymbol{u}, \tag{2.3}$$

$$\nabla \cdot \boldsymbol{u} = 0, \tag{2.4}$$

$$\mathrm{i}2(Pr/E)\sigma\Theta = \hat{\boldsymbol{z}} \cdot \boldsymbol{u} + \nabla^2\Theta, \tag{2.5}$$

where $\boldsymbol{u}$ is the three-dimensional velocity field, (u_s, u_ϕ, u_z), and σ is the half-frequency of inertial convection. In cylindrical coordinates, we may write solutions of the equations in the form

$$(u_s, u_\phi, u_z, \Theta)(s, \phi, z, t) = (u_s, u_\phi, u_z, \Theta)(s, z)\mathrm{e}^{\mathrm{i}(2\sigma t + m\phi)}, \tag{2.6}$$

where m is the azimuthal wavenumber which we assume to be positive. The wave propagates in the prograde direction when $\sigma < 0$ while it propagates in the retrograde direction when $\sigma > 0$. The temperature deviation from the purely conductive state, $T_0(z)$, is represented by Θ, and the non-dimensional physical parameters – the Rayleigh number R, the Prandtl number Pr and the Ekman number E – are defined as

$$R = \frac{\alpha\beta g d^2}{\Omega\kappa}, \quad Pr = \frac{\nu}{\kappa}, \quad E = \frac{\nu}{\Omega d^2}.$$

The geometric parameter is given by the aspect ratio Γ, defined as $\Gamma = s_0/d$. As in the previous studies (see, for example, Goldstein *et al.* 1993; Herrmann & Busse 1993), we shall assume perfectly conducting and stress-free conditions on the top and bottom of the cylinder, which permits separable solutions of the linear problem. We study inertial convection with four combinations of the boundary conditions on the sidewall of the cylinder:

(i) stress-free, impenetrable and perfectly conducting,

$$\frac{\partial}{\partial s}\left(\frac{u_\phi}{s}\right) = \frac{\partial u_z}{\partial s} = u_s = \Theta = 0 \quad \text{at} \quad s = \Gamma; \tag{2.7}$$

(ii) stress-free, impenetrable and perfectly insulating,

$$\frac{\partial}{\partial s}\left(\frac{u_\phi}{s}\right) = \frac{\partial u_z}{\partial s} = u_s = \frac{\partial \Theta}{\partial s} = 0 \quad \text{at} \quad s = \Gamma; \tag{2.8}$$

(iii) non-slip, impenetrable and perfectly conducting,

$$u_\phi = u_z = u_s = \Theta = 0 \quad \text{at} \quad s = \Gamma; \tag{2.9}$$

(iv) non-slip, impenetrable and perfectly insulating,

$$u_\phi = u_z = u_s = \frac{\partial \Theta}{\partial s} = 0 \quad \text{at} \quad s = \Gamma. \tag{2.10}$$

Equations (2.3)–(2.5) subject to any set of the boundary conditions in (2.7)–(2.10) form a convective stability problem which will be solved by both numerical and asymptotic analysis. It should be pointed out that the assumption of the stress-free top and bottom, leading to the separation of variables, dramatically simplifies the mathematical analysis of the problem. In this case, the z-dependence of the convection solution can be simply written as

$$u_\phi \sim \cos n\pi z, \quad u_z \sim \sin n\pi z, \quad u_s \sim \cos n\pi z, \quad \Theta \sim \sin n\pi z,$$

where n is a non-zero integer.

3. Numerical analysis

We expect convection in rapidly rotating cylinders to be non-axisymmetric (Goldstein *et al.* 1993). For the numerical analysis of the problem, a non-axisymmetric velocity vector satisfying equation (2.4) in cylindrical geometry can be expressed in terms of two scalar potentials Ψ and Φ (Marqués 1990)

$$\boldsymbol{u} = \frac{1}{s}\frac{\partial \Psi}{\partial \phi}\hat{\boldsymbol{s}} + \left(\frac{\partial \Phi}{\partial z} - \frac{\partial \Psi}{\partial s}\right)\hat{\boldsymbol{\phi}} - \frac{1}{s}\frac{\partial \Phi}{\partial \phi}\hat{\boldsymbol{z}}. \tag{3.1}$$

An important advantage of using (3.1) is that the two scalar potentials are decoupled for the velocity boundary condition on the stress-free or no-slip sidewall. In terms of Ψ and Φ, the stress-free velocity condition on the sidewall becomes

$$\Psi = \frac{\partial}{\partial s}\left(\frac{1}{s}\frac{\partial \Psi}{\partial s}\right) = \frac{\partial}{\partial s}\left(\frac{\Phi}{s}\right) = 0 \quad \text{at} \quad s = \Gamma, \tag{3.2}$$

while the non-slip velocity condition on the sidewall is imposed by

$$\Psi = \frac{\partial \Psi}{\partial s} = \Phi = 0 \quad \text{at} \quad s = \Gamma. \tag{3.3}$$

Making use of expression (3.1) and applying $\hat{\boldsymbol{z}}\cdot\nabla\times$ and $\hat{\boldsymbol{s}}\cdot\nabla\times$ on (2.3), we can derive the three independent non-dimensional scalar equations,

$$\left(\mathrm{i}2\sigma - E\nabla^2\right)\left[\frac{1}{s}\frac{\partial}{\partial s}\left(s\frac{\partial \Phi}{\partial z}\right) - \left(\nabla^2 - \frac{\partial^2}{\partial z^2}\right)\Psi\right] + \frac{2}{s}\frac{\partial^2 \Phi}{\partial z \partial \phi} = 0, \tag{3.4}$$

$$\left[\mathrm{i}2\sigma - E\left(\nabla^2 + \frac{2}{s}\frac{\partial}{\partial s} + \frac{1}{s^2}\right)\right]\left[\frac{\partial^2 \Psi}{\partial s \partial z} - \left(\nabla^2 - \frac{1}{s}\frac{\partial}{\partial s}s\frac{\partial}{\partial s}\right)\Phi\right]$$
$$- \frac{2}{s}\frac{\partial^2 \Psi}{\partial z \partial \phi} - \frac{2E}{s}\left[\frac{1}{s}\frac{\partial}{\partial s}\left(s\frac{\partial^2 \Phi}{\partial z^2}\right) - \left(\nabla^2 - \frac{\partial^2}{\partial z^2}\right)\frac{\partial \Psi}{\partial z}\right] - R\frac{1}{s}\frac{\partial \Theta}{\partial \phi} = 0, \tag{3.5}$$

$$[\nabla^2 - \mathrm{i}2\,(Pr/E)\,\sigma]\Theta - \frac{1}{s}\frac{\partial \Phi}{\partial \phi} = 0. \tag{3.6}$$

The convection problem is then solved numerically by using the Chebyshev-tau method in which the potential fields, Φ and Ψ, and the temperature deviation, Θ, are expanded in terms of the standard Chebyshev functions $T_k(x)$:

$$\left.\begin{aligned}
\Psi(s,z,\phi,t) &= s^m \left[\sum_{k=0}^{N+2} \hat{\Psi}_k \;\; T_k\left(\frac{2s}{\Gamma} - 1\right)\right] \cos(n\pi z)\exp \mathrm{i}(m\phi + 2\sigma t),\\
\Phi(s,z,\phi,t) &= s^{(m+1)} \left[\sum_{k=0}^{N+1} \hat{\Phi}_k \;\; T_k\left(\frac{2s}{\Gamma} - 1\right)\right] \sin(n\pi z)\exp \mathrm{i}(m\phi + 2\sigma t),\\
\Theta(s,z,\phi,t) &= s^m \left[\sum_{k=0}^{N+1} \hat{\Theta}_k \;\; T_k\left(\frac{2s}{\Gamma} - 1\right)\right] \sin(n\pi z)\exp \mathrm{i}(m\phi + 2\sigma t),
\end{aligned}\right\} \tag{3.7}$$

where $m \geqslant 1$, and $\hat{\Psi}_k$, $\hat{\Phi}_k$ and $\hat{\Theta}_k$ are complex coefficients. We shall take $n = 1$ in the numerical analysis because it always corresponds to the most unstable mode of convective instabilities. Note that the factors s^m and $s^{(m+1)}$ are imposed so that the expansion at the rotation axis $s = 0$ is regular. For numerical solutions with $E \geqslant O(10^{-5})$, we need to take $N = O(100)$ for an accuracy within 1%. Furthermore, the velocity boundary conditions on the sidewall $s = \Gamma$ must be enforced. For the stress-free boundary condition we require that

$$\left.\begin{aligned}
&\sum_{k=0}^{N+2} \hat{\Psi}_k = 0, \quad \sum_{k=0}^{N+1} (m + 2k^2)\hat{\Phi}_k = 0,\\
&\sum_{k=0}^{N+2} \left[m(m-2) + 2(2m-1)k^2 + \frac{4k^2}{3}(k^2 - 1)\right] \hat{\Psi}_k = 0;
\end{aligned}\right\} \tag{3.8}$$

and the non-slip boundary conditions demand that

$$\sum_{k=0}^{N+2} \hat{\Psi}_k = 0, \quad \sum_{k=0}^{N+1} \hat{\Phi}_k = 0, \quad \sum_{k=0}^{N+2} (m + 2k^2)\hat{\Psi}_k = 0. \tag{3.9}$$

The temperature condition on the sidewall is imposed in a similar way.

The primary purpose of our numerical analysis is to provide a valuable comparison with the results of the asymptotic analysis, which are valid only for small values of the Ekman number. The main results of the numerical analysis for inertial convection are shown in several tables below, together with those from the asymptotic analysis. In our numerical computations, we plotted nearly all the numerical solutions of inertial convection presented in the tables, demonstrating that the numerical solutions are almost identical to the corresponding asymptotic solutions. Hence, few of the figures from the numerical analysis are shown in the paper.

In the numerical analysis, we found that wall-localized convection is still preferred in a rapidly rotating cylinder when the Prandtl number Pr is sufficiently large. It is important to note that the wall-localized convection is marked by a very small half-frequency $\sigma_c = O(E)$ at $Pr = O(1)$ as well as critical values of R and m that are nearly independent of Pr. In contrast, inertial convection is marked by a high frequency and critical values of R and m that are strongly dependent on Pr. In

our numerical analysis, consequently, two different types of convection can be easily distinguished by their characteristics.

Since the focus of the present study is on inertial convection and the phenomenon of wall-localized convection is largely independent of cylindrical geometry, the rest of the paper will not discuss wall-localized convection in detail.

4. Asymptotic analysis for inertial convection

4.1. *Asymptotic solutions with stress-free sidewall*

A key assumption in the following asymptotic analysis is that the velocity field of inertial convection at leading order for $E \ll 1$ can be represented by a single inertial wave mode while buoyancy forces appear only at the next order to drive the inertial wave against the effects of viscous damping. This assumption allows a relatively simple asymptotic solution to be derived in rotating cylindrical systems. It leads to an asymptotic expansion in the form

$$\left.\begin{aligned} &\boldsymbol{u} = \boldsymbol{u}_0 + (\boldsymbol{u}_i + \boldsymbol{u}_b), \quad p = p_0 + (p_i + p_b), \\ &\sigma = \sigma_0 + \sigma_1, \quad \Theta = \Theta_0 + \cdots, \quad R = R_0 + \cdots, \end{aligned}\right\} \tag{4.1}$$

where $\boldsymbol{u}_i$ and p_i represent small perturbations to the leading-order solution $\boldsymbol{u}_0$ and p_0, and $\boldsymbol{u}_b$ and p_b denote perturbations in the Ekman boundary layer which are non-zero only in the vicinity of the sidewall of the cylinder. While $\boldsymbol{u}_i$ must be much smaller than the zeroth-order velocity $\boldsymbol{u}_0$, $|\boldsymbol{u}_i| \ll |\mathbf{u}_0|$, the boundary flow $\boldsymbol{u}_b$ has to be large enough so that $(\boldsymbol{u}_b + \boldsymbol{u}_0)$ satisfies the stress-free boundary condition on the sidewall. However, the instability problem can be solved without having to determine the detailed structure of the boundary-layer flow in the case of the stress-free sidewall. Clearly, two conditions must be satisfied for expansion (4.1): E must be sufficiently small, $E \ll 1$, and the modification of inertial-wave frequency by convection must be also small, i.e. $|\sigma_1/\sigma_0| \ll 1$.

After substitution of expansion (4.1) into equations (2.3)–(2.4), the perturbation solution $(\boldsymbol{u}_0, p_0, \sigma_0)$ at the zeroth order represents the inviscid inertial wave, the basic properties of which are discussed in the Appendix. The next-order problem in the asymptotic analysis is given by

$$2\,(\mathrm{i}\sigma_0 + \hat{\boldsymbol{z}}\times)\,(\boldsymbol{u}_i + \boldsymbol{u}_b) + \nabla(p_i + p_b) = R_0\hat{\boldsymbol{z}}\Theta_0 + E\nabla^2(\boldsymbol{u}_0 + \boldsymbol{u}_b) - \mathrm{i}2\sigma_1\boldsymbol{u}_0, \tag{4.2}$$

$$\nabla\cdot(\boldsymbol{u}_i + \boldsymbol{u}_b) = 0, \tag{4.3}$$

$$(\nabla^2 - \mathrm{i}2\sigma_0 E^{-1}Pr)\Theta_0 = -\hat{\boldsymbol{z}}\cdot\boldsymbol{u}_0. \tag{4.4}$$

Two key features should be noted in the above equations. Physically, thermal effects are coupled with an inertial wave mode at this order, driving inertial convection against viscous dissipation. Mathematically, the inhomogeneous differential equation (4.2) requires a solvability condition whose real part yields the Rayleigh number for the onset of convection and whose imaginary part gives rise to a small correction of the half-frequency of the inertial wave σ_0.

An asymptotic solution of inertial convection contains three major elements. The first is the asymptotic expression for the Rayleigh number R_0 at the onset of convection. Denoting the complex conjugate of $\boldsymbol{u}_0$ by $\boldsymbol{u}_0^*$, which also satisfies $\nabla\cdot\boldsymbol{u}_0^* = 0$, and making use of

$$\langle\boldsymbol{u}_0^*\cdot\nabla(p_i + p_b)\rangle_V = 0, \tag{4.5}$$

$$\langle \boldsymbol{u}_0^* \cdot (\mathrm{i}\sigma_o + \hat{\boldsymbol{z}}\times)(\boldsymbol{u}_i + \boldsymbol{u}_b)\rangle_V = 0, \tag{4.6}$$

where $\langle\,\rangle_V$ denotes the volume integral over the cylinder, we can derive the solvability condition for equation (4.2), the real part of which gives rise to the Rayleigh number R_0:

$$R_0 = \left\{ \frac{\langle|\nabla \times \boldsymbol{u}_0|^2\rangle_V - (2/\Gamma)\langle|\hat{\boldsymbol{\phi}} \cdot \boldsymbol{u}_0|^2\rangle_S}{\mathrm{Re}[\langle \boldsymbol{u}_0^* \cdot \hat{\boldsymbol{z}}\Theta_0\rangle_V]} \right\} E, \tag{4.7}$$

where $\langle\,\rangle_S$ represents the surface integral over the sidewall of the cylinder. While analytical expressions can be derived in closed form for $\langle|\nabla \times \boldsymbol{u}_0|^2\rangle_V$ and $\langle|\hat{\boldsymbol{\phi}} \cdot \boldsymbol{u}_0|^2\rangle_S$, the solution Θ_0 of the inhomogeneous heat equation (4.4) with a given $\hat{\boldsymbol{z}} \cdot \boldsymbol{u}_0$ on its right-hand side cannot be found in closed form. The only way to solve (4.4) conveniently is through an expansion of Θ_0 in terms of the Bessel functions with analytic coefficients. For the conducting sidewall, we can write

$$\Theta_0 = -\frac{2[J_m(\xi)]^2\sigma_0}{\pi^2} \times \sum_{k=1}^{K} \left[\mathrm{i}\left(\pi^2 + \beta_k^2/\Gamma^2\right) + 2\sigma_0 Pr/E\right] \hat{\gamma}_k J_m(s\beta_k/\Gamma) \sin \pi z \mathrm{e}^{\mathrm{i}(m\phi + 2\sigma_0 t)}, \tag{4.8}$$

where $J_m(x)$ denotes the standard Bessel function,

$$\hat{\gamma}_k = \frac{\pi^3 \Gamma^2 \beta_k^2}{2\sigma_0^2\left(\xi^2 - \beta_k^2\right)^2\left[\left(\pi^2 + \beta_k^2/\Gamma^2\right)^2 + (2\sigma_0 Pr/E)^2\right]}, \tag{4.9}$$

$$\xi = (\pi\Gamma)\sqrt{\frac{1-\sigma_0^2}{\sigma_0^2}}, \tag{4.10}$$

and β_k is chosen such that

$$J_m(\beta_k) = 0, \quad 0 < \beta_1 < \beta_2 < \beta_3 < \cdots .$$

It is significant to note that only a small number of terms in (4.8) is usually needed in the expansion. For instance, three terms ($K = 3$) yield a solution such that the Rayleigh number and the frequency at the onset of convection are accurate within 3%. For the insulating sidewall, we obtain

$$\Theta_0 = -\frac{2\sigma_0[\xi J_{m+1}(\xi) - m J_m(\xi)]^2}{\pi^2\left(\beta_k^2 - m^2\right)} \times \sum_{k=1}^{K} \left[\mathrm{i}\left(\pi^2 + \beta_k^2/\Gamma^2\right) + 2\sigma_0 Pr/E\right] \hat{\gamma}_k J_m(s\beta_k/\Gamma) \sin \pi z \mathrm{e}^{\mathrm{i}(m\phi + 2\sigma_0 t)}, \tag{4.11}$$

where $\hat{\gamma}_k$ has the same form as that given in (4.9) except that β_k are now the roots of the equation

$$\beta_k J_{m+1}(\beta_k) - m J_m(\beta_k) = 0, \quad 0 < \beta_1 < \beta_2 < \beta_3 < \cdots .$$

In the case of the boundary condition (2.7), the asymptotic expression for the Rayleigh number R_0 is given by the real part of the solvability condition,

$$R_0 = \left\{ \frac{2\Gamma^2\pi^2\left(1-\sigma_0^2\right)^2 I_V(m) - \sigma_0^2\pi\left[\xi J_{m-1}(\xi) + m(\sigma_0-1)J_m(\xi)\right]^2}{2\Gamma^2\left[J_m(\xi)\right]^2\sigma_0^2\left(1-\sigma_0^2\right)^2\left[\sum_{k=1}^{K}\left(\pi^2+\beta_k^2/\Gamma^2\right)\hat{\gamma}_k\right]} \right\} E, \qquad (4.12)$$

where the property (1.2) in the dimensionless form is used $\hat{\gamma}_k$ is given by the analytical expression (4.9) and

$$I_V(m) = \frac{\pi}{16}\left[\frac{q_{m-1}}{(1-\sigma_0)^2} + \frac{q_{m+1}}{(1+\sigma_0)^2} + \frac{2\pi^2\Gamma^2 q_m}{\xi^2\sigma_0^2}\right],$$
$$q_j = \left[j J_j(\xi) - \xi J_{j+1}(\xi)\right]^2 + (\xi^2 - j^2)\left[J_j(\xi)\right]^2.$$

Physically we are interested in the smallest Rayleigh number R_0, denoted by R_c, at which convective instability can occur. However, the process of determining the most unstable mode should be contrasted with ordinary convection problems such as the Rayleigh–Bénard problem. In the present problem, it is not a question of finding a wavenumber m that minimizes R_0, but of determining the three-dimensional structure of the flow as well as its approximate oscillation frequency by minimizing R_0 in (4.12) over different inertial wave modes.

An asymptotic solution for inertial convection is then obtained by the following procedure. First, we minimize the expression of R_0 by inserting into (4.12) different inertial wave modes, such as those given in table 8. After determining on the basis of (4.12) the critical Rayleigh number R_c, the critical wavenumber m_c and the corresponding σ_0 (or l), we take the imaginary part of the solvability condition to calculate the critical half-frequency, which corresponds to the second major element in the asymptotic solution:

$$\sigma_c = \sigma_0 - \left\{ \frac{\sigma_0\left[J_{m_c}(\xi)\right]^2(R_c/E)}{I_V(m_c)} \left(\sum_{k=1}^{K}\hat{\gamma}_k\right) \right\} Pr, \qquad (4.13)$$

where the analytical expression for $\hat{\gamma}_k$ is again given by (4.9). Evidently, the effect of convection is always to reduce the frequency of a purely inertial wave mode. Moreover, the asymptotic expression is not valid when $Pr = O(1)$, for which inertial convection is no longer preferred. The third major element in the asymptotic solution is the leading-order velocity of the convection, the inviscid inertial wave (A 13)–(A 15) given in the Appendix. Expressions (4.8), (4.12)–(4.13) and (A 13)–(A 15) represent an asymptotic solution of inertial convection in a rotating cylinder satisfying the condition (2.7) for an arbitrary aspect ratio Γ.

It is profitable to examine the asymptotic scaling at small Pr before discussing the detailed asymptotic and numerical results. Let us look at two different ranges of Pr for a given small but non-zero E. In the first range $0 < Pr \ll E$, the coefficients $\hat{\gamma}_k$ are $O(1)$ for a given value of the wavenumber $l = O(1)$ and $m = O(1)$. Expression (4.12) then gives $R_0 = O(E)$ independent of Pr while (4.13) shows that the deviation from the inertial wave frequency is $O(Pr)$. The second range is $Pr \gg E$, say, $Pr = O(E^{1/2})$. In this case, the coefficients $\hat{\gamma}_k$ are $O((E/Pr)^2)$, expression (4.12) gives $R_0 = O(Pr^2/E)$ while (4.13) indicates that the deviation from σ_0 is also $O(Pr)$. In figure 1, we illustrate several typical examples showing how the Rayleigh number R_0 is dependent

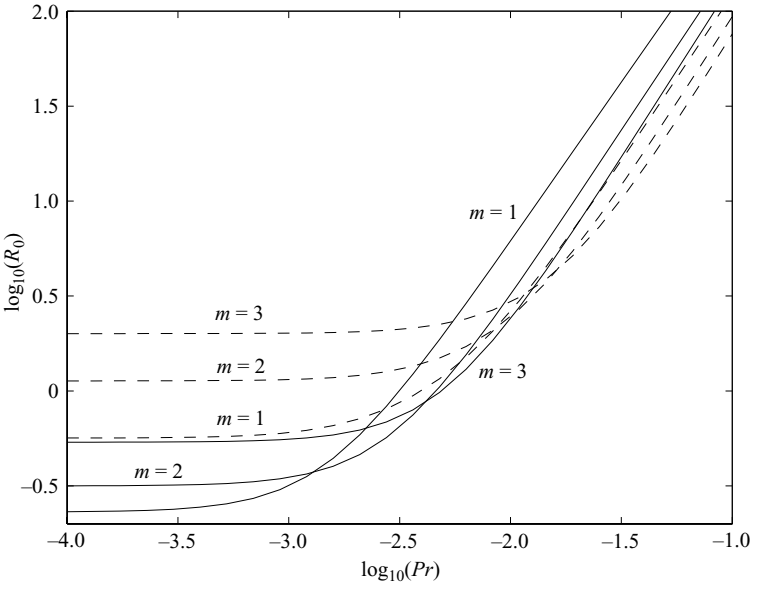

FIGURE 1. The value of R_0 is shown as a function of Pr for $E = 10^{-4}$ over different inertial modes according to (4.12). Solid lines represent the inertial modes with $l = 1$ and dashed lines the $l = 2$ modes. The sidewall of the cylinder is stress-free and conducting.

Pr	l	m_c	$(R_c, \sigma_c)_{asymptotic}$	$(R_c, \sigma_c)_{numerical}$
0	1	1	(0.230, 0.781)	(0.230, 0.781)
0.0025	1	2	(0.524, 0.607)	(0.523, 0.607)
0.005	1	3	(1.021, 0.490)	(1.017, 0.490)
0.01	2	4	(2.234, 0.410)	(2.216, 0.410)
0.025	2	3	(7.260, 0.325)	(7.145, 0.325)
0.05	3	5	(17.66, 0.246)	(17.16, 0.247)
0.1	3	4	(44.04, 0.184)	(42.02, 0.185)

TABLE 1. Several critical parameters at the onset of convection for different Prandtl numbers in a rotating cylinder with a stress-free and conducting sidewall for $E = 10^{-4}$ and $\Gamma = 1$. The integer l indicates the radial structure of inertial convection. Both the fully numerical and asymptotic solutions are shown.

on different inertial modes with increasing Pr. It suggests that the Rayleigh number R_0 is nearly independent of Pr in the range $0 < Pr \ll E$ while a slope of about 2 in the range $Pr = O(E^{1/2})$ is evident on the right-hand side of the figure. We shall discuss the Pr-dependence further in § 4.3.

Several typical critical parameters for $\Gamma = 1$ and $E = 10^{-4}$, calculated from both the asymptotic expressions and the full numerical solution, are shown in table 1. The index l, indicating the radial structure of the convective flow, is also shown in the table. It is worth noting that, though a sum over $\hat{\gamma}_k$ appears in the expressions, the number of terms required in (4.12)–(4.13) is rather small. For example, three terms ($K = 3$) give $R_c = 7.52, \sigma_c = 0.325$ for $\Gamma = 1$ and $Pr = 0.025$ while an asymptotically large $K(\gg 1)$ yields $R_c = 7.26, \sigma_c = 0.325$. The asymptotic solution

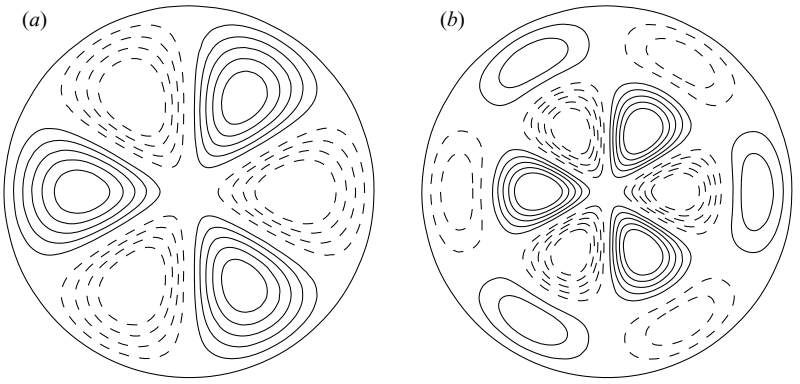

FIGURE 2. Contours of u_s two asymptotic solutions in a horizontal plane for $\Gamma = 1$ and $E = 10^{-4}$: (*a*) $Pr = 0.005$ with the critical parameters $m_c = 3$, $R_c = 1.021$, $\sigma_c = 0.490$ and (*b*) $Pr = 0.025$ with $m_c = 3$, $R_c = 7.26$, $\sigma_c = 0.325$. The sidewall of the cylinder is stress-free and conducting.

shows a quantitative agreement with the fully numerical solution for all $Pr \leqslant O(0.1)$. An important feature of inertial convection in a rotating cylinder is that the critical wavenumber m_c does not generally increase with increasing Pr as in the case of spherical geometry. This is due to the fact that different values of σ_0 correspond to different radial structures of the convective motion. Various combinations of the azimuthal and radial structure, dependent upon the size of Pr, can achieve the most unstable state of convection. In this sense, the dynamics of convection and its pattern selection in a rotating cylinder are richer than in other systems such as a rotating sphere. The selection process is clearly illustrated in figure 1. For instance, convection selects the inertial mode with $m_c = 3$ and $l = 1$ at $\log_{10} Pr = \log_{10} 0.005 = -2.3$ while the mode with $m_c = 3$ and $l = 2$ becomes preferred at $\log_{10} Pr = \log_{10} 0.025 = -1.60$. Figure 2 shows the spatial structure of two asymptotic solutions for a rotating cylinder with $\Gamma = 1$ at $E = 10^{-4}$ for $Pr = 0.005$ and $Pr = 0.025$. Though both the solutions have the same critical wavenumber $m_c = 3$, the radial structures are quite different. The solution for $\sigma_c = 0.490$ ($l = 1$) and $Pr = 0.005$ has one radial layer, while two radial layers ($l = 2$) are exhibited by the solution with $\sigma_c = 0.325 (l = 2)$ and $Pr = 0.025$.

Since the radial structure represents a key feature of inertial convection, it is of interest to look at the effect of larger aspect ratios, which allow a more complex radial structure in the flow. Several typical critical parameters of inertial convection for $E = 10^{-4}$ with $\Gamma = 2$, calculated from both the asymptotic expressions and full numerics, are displayed in table 2. This again shows an irregular dependence of the critical wavenumber m_c on the Prandtl number Pr. Two asymptotic solutions for inertial convection in a cylinder with $\Gamma = 2$ at $E = 10^{-4}$ are shown in figure 3 for $Pr = 0.01$ and $Pr = 0.05$. These two asymptotic solutions have the same critical wavenumber $m_c = 10$, but there is a single radial layer for the solution with $\sigma_c = 0.408 (l = 1)$ and $Pr = 0.01$, while there are four radial layers for $\sigma_c = 0.232 (l = 4)$ and $Pr = 0.05$.

When the sidewall of a cylinder is subject to the stress-free and insulating condition given by (2.8), the asymptotic analysis can be carried out in the same way, yielding

Pr	l	m_c	$(R_c, \sigma_c)_{asymptotic}$	$(R_c, \sigma_c)_{numerical}$
0	1	1	(0.159, −0.778)	(0.159, −0.778)
0.0025	1	5	(0.516, 0.621)	(0.515, 0.621)
0.005	1	7	(1.048, 0.516)	(1.044, 0.516)
0.01	1	10	(2.345, 0.408)	(2.331, 0.408)
0.025	1	15	(7.394, 0.298)	(7.306, 0.298)
0.05	4	10	(18.08, 0.233)	(17.72, 0.233)
0.1	5	12	(44.98, 0.180)	(43.17, 0.180)

TABLE 2. Several critical parameters at the onset of convection for different Prandtl numbers in a rotating cylinder with the stress-free and conducting sidewall for $E = 10^{-4}$ and $\Gamma = 2$. Both the fully numerical and asymptotic solutions are shown.

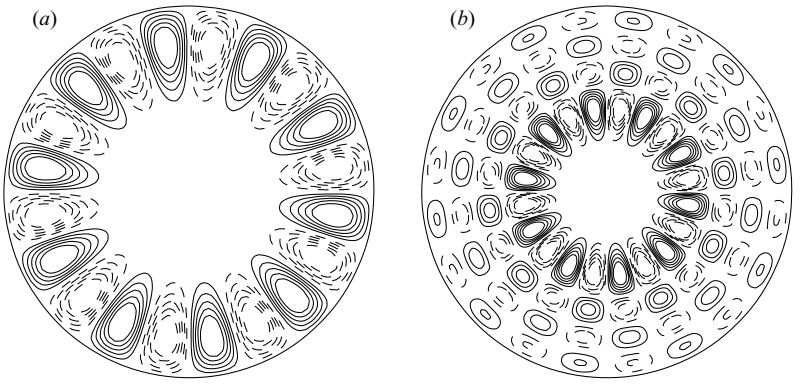

FIGURE 3. Contours of u_s for the asymptotic solutions in a horizontal plane for $\Gamma = 2$ and $E = 10^{-4}$: (*a*) $Pr = 0.01$ with the critical parameters $m_c = 10$, $R_c = 2.345$, $\sigma_c = 0.408$ and (*b*) $Pr = 0.05$ with $m_c = 10$, $R_c = 18.08$, $\sigma_c = 0.233$. The sidewall of the cylinder is stress-free and conducting.

an asymptotic expression for the Rayleigh number R_0:

$$R_0 = \left\{ \frac{2\Gamma^2\pi^2\left(1-\sigma_0^2\right)^2 I_V(m) - \sigma_0^2\pi\left[\xi J_{m-1}(\xi) + m(\sigma_0 - 1)J_m(\xi)\right]^2}{2\Gamma^2\left[\xi J_{m+1}(\xi) - m J_m(\xi)\right]^2 \sigma_0^2\left(1-\sigma_0^2\right)^2 \left[\sum_{k=1}^{K} \frac{\left(\pi^2 + \beta_k^2/\Gamma^2\right)}{\left(\beta_k^2 - m^2\right)}\hat{\gamma}_k\right]} \right\} E, \quad (4.14)$$

where the analytical expression for $\hat{\gamma}_k$ is again given by (4.9). After determining the values of R_c, σ_0 and m_c through (4.14) we calculate the corresponding critical half-frequency σ_c,

$$\sigma_c = \sigma_0 - \left\{ \frac{\sigma_0 (R_c/E)\left[\xi J_{m_c+1}(\xi) - m J_{m_c}(\xi)\right]^2}{I_V(m_c)} \right\} \left(\sum_{k=1}^{K} \frac{\hat{\gamma}_k}{\beta_k^2 - m^2} \right) Pr. \quad (4.15)$$

The leading-order velocity for inertial convection is still given by (A 13)–(A 15). Expressions (4.11), (4.14)–(4.15) as well as (A 13)–(A 15) represent the asymptotic solution for inertial convection in a rapidly rotating cylinder ($E \ll 1$) satisfying the condition (2.8) for an arbitrary aspect ratio Γ. Several typical critical parameters of inertial convection for $E = 10^{-4}$ and $\Gamma = 1$ are shown in table 3. It is particularly

Pr	l	m_c	$(R_c, \sigma_c)_{asymptotic}$	$(R_c, \sigma_c)_{numerical}$
0	1	1	(0.103, 0.781)	(0.102, 0.781)
0.0025	1	3	(0.503, 0.490)	(0.502, 0.490)
0.005	1	4	(1.110, 0.411)	(1.110, 0.411)
0.01	2	2	(2.459, 0.387)	(2.442, 0.387)
0.025	3	2	(7.694, 0.276)	(7.634, 0.276)
0.05	4	1	(18.90, 0.239)	(18.33, 0.239)
0.1	5	1	(46.66, 0.181)	(44.25, 0.182)

TABLE 3. Several critical parameters at the onset of convection for different Prandtl numbers in a rotating cylinder with a stress-free and insulating sidewall for $E = 10^{-4}$ and $\Gamma = 1$. Both the fully numerical and analytical solutions are shown.

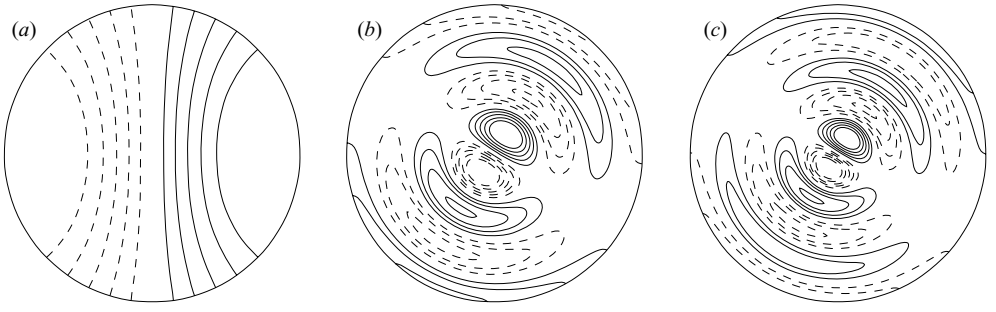

FIGURE 4. Contours of Θ_0 for three asymptotic solutions in the middle plane ($z = 0.5$) for a cylinder with $\Gamma = 1$ at $E = 10^{-4}$: (*a*) $Pr = 0$ with $m_c = 1$, $R_c = 0.103$, $\sigma_c = 0.781$, (*b*) $Pr = 0.05$ with $m_c = 1$, $R_c = 18.90$, $\sigma_c = 0.239$ and (*c*) $Pr = 0.1$ with $m_c = 1$, $R_c = 46.6$, $\sigma_c = 0.181$. The sidewall of the cylinder is stress-free and insulating.

interesting to compare the structures of the three asymptotic solutions with the same wavenumber $m_c = 1$ for different values of Pr. The temperature fields Θ_0 of the three solutions with $\Gamma = 1$ are depicted in figure 4 for $Pr = 0, 0.05, 0.1$ at $E = 10^{-4}$. They illustrate how the effect of the Prandtl number alters the radial structure of convection: from the simplest radial structure at $Pr = 0$ to the five radial-layer pattern at $Pr = 0.1$. When the Prandtl number increases further $Pr > O(0.1)$, the inertial mode no longer represents the preferred form of convection. We will be discuss the transition from inertial to wall-localized convection later in § 4.3.

4.2. *Asymptotic solutions with a rigid sidewall*

The asymptotic analysis in a rigid-sidewall cylinder is slightly more complicated because the Ekman boundary layer cannot be treated implicitly in terms of a surface integral as in the case of a stress-free sidewall. For the interior flow of inertial convection, we assume the following perturbation expansion for $E \ll 1$:

$$\left.\begin{aligned} &\boldsymbol{u} = \boldsymbol{u}_0 + \boldsymbol{u}_1, \quad p = p_0 + p_1, \\ &\sigma = \sigma_0 + \sigma_1, \quad \Theta = \Theta_0 + \cdots, \quad R = R_0 + \cdots, \end{aligned}\right\} \tag{4.16}$$

where $\boldsymbol{u}_1$ and p_1 represent the perturbation of the interior solution. We also make a similar expansion for the Ekman boundary layer in the vicinity of the rigid sidewall at $s = \Gamma$:

$$\boldsymbol{u}_b = \tilde{\boldsymbol{u}}_0 + \tilde{\boldsymbol{u}}_1, \quad p_b = \tilde{p}_0 + \tilde{p}_1, \tag{4.17}$$

where $\boldsymbol{u}_b$ is the Ekman boundary-layer flow and $\tilde{\boldsymbol{u}}_0 = O(1), \tilde{\boldsymbol{u}}_1 = O(E^{1/2})$. After substitution of expansion (4.16) into (2.3)–(2.5), the zeroth order of the interior problem is the same as that for the stress-free sidewall given by (A 1)–(A 2). The governing equations for the perturbation of the interior flow are

$$\mathrm{i}2\sigma_o \boldsymbol{u}_1 + 2\hat{\boldsymbol{z}} \times \boldsymbol{u}_1 + \nabla p_1 = R_0 \hat{\boldsymbol{z}} \Theta_0 + E\nabla^2 \boldsymbol{u}_0 - \mathrm{i}2\sigma_1 \boldsymbol{u}_0, \tag{4.18}$$

$$\nabla \cdot \boldsymbol{u}_1 = 0. \tag{4.19}$$

$$(\nabla^2 - \mathrm{i}2\sigma_o E^{-1} Pr)\Theta_0 = -\hat{\boldsymbol{z}} \cdot \boldsymbol{u}_0, \tag{4.20}$$

where we have kept the term, $E\Delta^2 \boldsymbol{u}_0$, for the interior dissipation which is, as we will show later, of the same order of magnitude as that for the boundary-layer dissipation. Because of the rigid sidewall, (4.6) is no longer valid. Instead, the volume integral becomes

$$\langle \boldsymbol{u}_0^* \cdot (\mathrm{i}2\sigma_0 \boldsymbol{u}_1 + 2\mathbf{k} \times \boldsymbol{u}_1) \rangle_V = \Gamma \int_0^1 \int_0^{2\pi} p_0^* \hat{\boldsymbol{s}} \cdot \boldsymbol{u}_1 \mathrm{d}\phi \, \mathrm{d}z \tag{4.21}$$

on the sidewall, and $\hat{\boldsymbol{s}} \cdot \boldsymbol{u}_1$ must be matched to the flux from the Ekman boundary layer at the sidewall.

After a straightforward analysis for the Ekman boundary layer on the sidewall, which provides the matching condition for (4.21), a solvability condition for the inhomogeneous differential equation (4.18) can be readily derived. For a conducting sidewall, the real part of the solvability condition yields the Rayleigh number for the onset of convection:

$$R_0 = \frac{4\Gamma\pi^2 I_V(m) b^2 E + \sqrt{|\sigma_0|}\left\{\pi\sigma_0^2 \left[\xi J_{m-1}(\xi) + m(\sigma_0 - 1) J_m(\xi)\right]^2 + \Gamma^2 b^2 \pi^3 [J_m(\xi)]^2\right\} E^{1/2}}{4\Gamma\sigma_0^2 b^2 [J_m(\xi)]^2 \left[\sum_{k=1}^{K} \left(\pi^2 + \beta_n^2/\Gamma^2\right) \hat{\gamma}_k\right]}, \tag{4.22}$$

where $b^2 = (1 - \sigma_0^2)^2$ and the analytical expression for $\hat{\gamma}_k$ is given by (4.9). The first term in the numerator of (4.22), proportional to E, represents the effect of the internal viscous dissipation. The second term in the numerator of (4.22), proportional to $E^{1/2}$, results from the Ekman boundary-layer flux on the sidewall given by (4.21), representing the effect of the boundary-layer viscous dissipation.

To determine the critical Rayleigh number R_c, the associated critical wavenumber m_c and leading-order half-frequency σ_0 we first minimize R_0 as given by (4.22) with respect to different three-dimensional inertial modes. We then use the imaginary part of the solvability condition to determine the critical half-frequency, σ_c, the second element in the asymptotic solution:

$$\sigma_c = \sigma_0 - \frac{\sigma_0 (R_c/E)[J_{m_c}(\xi)]^2}{I_V(m_c)} \left(\sum_{k=1}^{K} \hat{\gamma}_k\right) Pr - \frac{\sigma_0}{8 I_V(m_c)\sqrt{|\sigma_0|}} \times \left\{\frac{\pi}{b^2\Gamma}\left[\xi J_{m_c - 1}(\xi) + m_c(\sigma_0 - 1) J_{m_c}(\xi)\right]^2 + \frac{\Gamma\pi^3}{\sigma_0^2}[J_{m_c}(\xi)]^2\right\} E^{1/2}. \tag{4.23}$$

It is important to note that, while it appears that the two terms in the numerator of (4.22) are of quite different orders of magnitude in the limit $E \ll 1$, they are of the same order of magnitude for the convection mode minimizing R_0 at small, but finite values of Pr. This is caused by the fact that we have not denoted explicitly the E-dependence of the minimizing wavenumber nor that of the corresponding frequency

σ_c. In this connection it is of interest to look at the oscillatory instability in a rapidly rotating ($E \ll 1$) unbounded ($\Gamma \to \infty$) Bénard layer with two stress-free horizontal bounding surfaces. Because of the absence of sidewalls we can minimize the Rayleigh number with respect to the total horizontal wavenumber, $a^2 = a_x^2 + a_y^2$, which yields for the critical wavenumber a_c:

$$a_c \sim (\sqrt{2}\pi Pr)^{1/3}\ E^{-1/3} \quad \text{as} \quad E \to 0, \tag{4.24}$$

for a fixed small Prandtl number $0 < Pr \ll 1$. By inserting (4.24) into the corresponding expressions for the critical Rayleigh number and half-frequency, we can obtain the asymptotic expressions for the critical values of R_c and σ_c:

$$R_c \sim 6(\sqrt{2}\pi Pr)^{4/3}\ E^{-1/3}, \tag{4.25}$$

$$\sigma_c \sim \frac{\sqrt{2}}{2}(\sqrt{2}\pi Pr^{-1})^{2/3}\ E^{1/3}, \tag{4.26}$$

valid for $E \ll 1$ at a fixed small Pr. The interior viscous dissipation of this solution is of the order $EE^{-2/3}$, while the contribution from the Ekman layer at the sidewall is of the order $\Gamma E E^{-1/3}/\delta_E$, where δ_E is the Ekman layer thickness which for motions with the frequency σ_c is of the order $E^{1/3}$. For aspect ratios Γ of the order unity we thus find that the two contributions are of the same order of magnitude in the limit $E \ll 1$ at a fixed small Pr. The next-order term neglected in (4.22), which involves the $O(E^{1/2})$ secondary flows in both the Ekman layer and the interior, would be of the order $E^{1/2}$ smaller than that given by (4.22).

The third element in the asymptotic solution, the corresponding velocity of leading-order inertial convection, is given in the complex form by

$$\hat{\boldsymbol{s}} \cdot \boldsymbol{u} = \frac{-\mathrm{i}\cos \pi z}{2\left(1-\sigma_0^2\right)} \left[\frac{\sigma_0 \xi}{\Gamma} J_{m_c-1}\left(\frac{\xi s}{\Gamma}\right) + \frac{m_c(1-\sigma_0)}{s} J_{m_c}\left(\frac{\xi s}{\Gamma}\right) \right] \mathrm{e}^{\mathrm{i}(m_c\phi + 2\sigma_0 t)}, \tag{4.27}$$

$$\begin{aligned} \hat{\boldsymbol{\phi}} \cdot \boldsymbol{u} = \frac{\cos \pi z}{2\left(1-\sigma_0^2\right)} \Bigg\{ & \left[\frac{\xi}{\Gamma} J_{m_c-1}\left(\frac{\xi s}{\Gamma}\right) - \frac{m_c(1-\sigma_0)}{s} J_{m_c}\left(\frac{\xi s}{\Gamma}\right) \right] \\ & - \left[\frac{\xi}{\Gamma} J_{m_c-1}(\xi) - \frac{m_c(1-\sigma_0)}{s} J_{m_c}(\xi) \right] \mathrm{e}^{-\gamma(\Gamma - s)} \Bigg\} \mathrm{e}^{\mathrm{i}(m_c\phi + 2\sigma_0 t)}, \end{aligned} \tag{4.28}$$

$$\hat{\boldsymbol{z}} \cdot \boldsymbol{u} = \frac{-\mathrm{i}\pi \sin \pi z}{2\sigma_0} \left[J_{m_c}\left(\frac{\xi s}{\Gamma}\right) - J_{m_c}(\xi)\, \mathrm{e}^{-\gamma(\Gamma - s)} \right] \mathrm{e}^{\mathrm{i}(m_c\phi + 2\sigma_0 t)}, \tag{4.29}$$

with $\gamma = \sqrt{|\sigma_0|/E}\ (1 + \mathrm{i}\sigma_0/|\sigma_0|)$. Several typical critical parameters of inertial convection for $E = 10^{-4}$, calculated from both the asymptotic expressions and full numerics, are shown in table 4 for the rigid and conducting sidewall with different values of Pr.

In figure 5, we show the spatial structure of two asymptotic solutions in a rotating cylinder with $\Gamma = 1$ at $E = 10^{-4}$ for $Pr = 0.005$ and $Pr = 0.025$. While the solution for $Pr = 0.005$ has the critical wavenumber $m_c = 3$, the solution for $Pr = 0.025$ has $m_c = 7$. But both the solutions have a similar two-radial-layer structure.

Pr	l	m_c	$(R_c, \sigma_c)_{asymptotic}$	$(R_c, \sigma_c)_{numerical}$
0	1	1	(0.763, 0.779)	(0.753, 0.779)
0.0025	1	2	(1.603, −0.455)	(1.607, −0.455)
0.005	1	3	(2.515, 0.485)	(2.522, 0.484)
0.01	1	5	(4.320, 0.350)	(4.326, 0.349)
0.025	1	7	(10.49, 0.271)	(10.46, 0.271)
0.05	2	6	(22.57, 0.217)	(22.24, 0.217)
0.1	3	6	(51.09, 0.164)	(49.71, 0.164)

TABLE 4. Several critical parameters at the onset of convection for different Prandtl numbers in a rotating cylinder with $\Gamma = 1$ and $E = 10^{-4}$. Both the fully numerical and asymptotic solutions are shown. The sidewall of the cylinder is rigid and conducting.

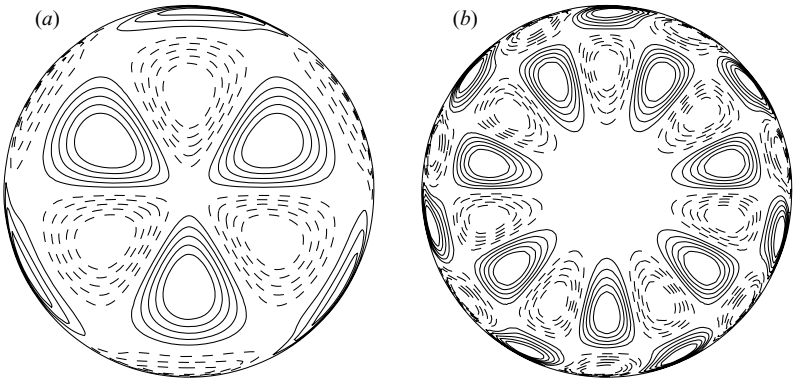

FIGURE 5. Contours of u_ϕ for two asymptotic solutions at $z = 0.25$ for a cylinder with $\Gamma = 1$ at $E = 10^{-4}$: (*a*) $Pr = 0.005$ with the critical parameters $m_c = 3$, $R_c = 2.515$, $\sigma_c = 0.485$ and (*b*) $Pr = 0.025$ with $m_c = 7$, $R_c = 10.49$, $\sigma_c = 0.271$. The sidewall of the cylinder is rigid and conducting.

In the case of an insulating sidewall, a similar asymptotic analysis for inertial convection can be carried out, which gives

$$R_0 = \frac{4\Gamma\pi^2 I_V(m) b^2 E + \sqrt{|\sigma_0|}\left\{\pi\sigma_0^2\left[\xi J_{m-1}(\xi) + m(\sigma_0 - 1)J_m(\xi)\right]^2 + \Gamma^2 b^2 \pi^3 J_m^2(\xi)\right\} E^{1/2}}{4\Gamma\sigma_0^2 b^2 \left[\xi J_{m+1}(\xi) - m J_m(\xi)\right]^2 \left[\sum_{k=1}^{K} \frac{\left(\pi^2 + \beta_k^2/\Gamma^2\right)}{\left(\beta_k^2 - m^2\right)} \hat{\gamma}_k\right]}. \tag{4.30}$$

This determines the critical Rayleigh number R_c, the critical wavenumber m_c and the leading-order half-frequency σ_0. The critical half-frequency σ_c is then given by

$$\sigma_c = \sigma_0 - \frac{\sigma_0 (R_c/E)\left[\xi J_{m_c+1}(\xi) - m_c J_{m_c}(\xi)\right]^2}{I_V(m_c)} \left(\sum_{k=1}^{K} \frac{\hat{\gamma}_k}{\beta_k^2 - m^2}\right) Pr - \frac{\sigma_0}{8 I_V(m_c)\sqrt{|\sigma_0|}}$$
$$\times \left\{\frac{\pi}{b^2\Gamma}\left[\xi J_{m_c-1}(\xi) + m_c(\sigma_0 - 1)J_{m_c}(\xi)\right]^2 + \frac{\Gamma\pi^3}{\sigma_0^2}\left[J_{m_c}(\xi)\right]^2\right\} E^{1/2}. \tag{4.31}$$

Before discussing the detailed result, we first look at the asymptotic scaling at small Pr. Similar to what was discussed in the preceding section, we consider two different ranges of Pr for a given small but non-zero E. In the first range $0 < Pr \ll E$, the

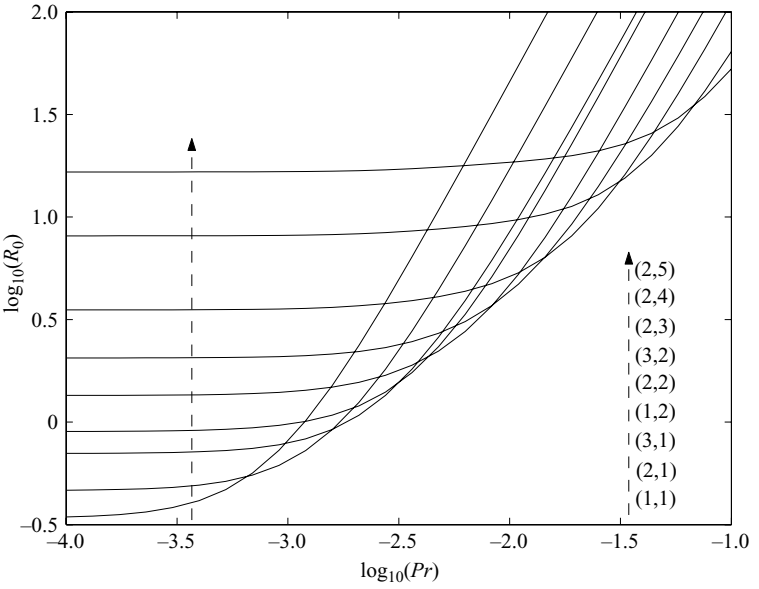

FIGURE 6. The Rayleigh number R_0 is shown as a function of Pr for different inertial modes according to (4.30) for $E = 10^{-4}$. The first number in the bracket denotes the azimuthal wavenumber m while the second number is l relating to the radial structure of inertial convection. The sidewall of the cylinder is rigid and insulating and $\Gamma = 1$.

coefficients $\hat{\gamma}_k$ are $O(1)$ for a given value of the wavenumber $l = O(1)$ and $m = O(1)$. Expression (4.30) gives $R_0 = O(E^{1/2})$ while (4.31) indicates that the deviation from the inviscid half-frequency σ_0 is $O(E^{1/2})$. In the second range $Pr = O(E^{1/2})$, the coefficients $\hat{\gamma}_k$ are $O((E/Pr)^2)$, expression (4.30) gives $R_0 = O(Pr^2/E^{3/2})$ while (4.31) shows that the deviation from σ_0 is $O(Pr/E^{1/2})$. In this simple scaling estimate, we have assumed that $l = O(1)$ and $m = O(1)$ which is of course not generally correct at the onset of convection. The Pr-dependence of the problem is quite complicated and will be discussed further in § 4.3.

A typical selection process for the convection pattern is illustrated in figure 6, showing how R_0 is dependent on different inertial modes in a rotating cylinder with a rigid sidewall. Generally speaking, (l^2+m^2) increases monotonically with increasing Pr when either the radial scale or the azimuthal scale or both decrease. For example, for $\log_{10} Pr = \log_{10}(0.025) = -1.6$, the convection system selects the inertial mode with $m_c = 2$ and $l = 3$, while the inertial mode with $m_c = 2$ but $l = 4$ becomes preferred at $\log_{10} Pr = \log_{10}(0.05) = -1.30$. When Pr increases to $\log_{10} Pr = \log_{10}(0.1) = -1.0$, the preferred convection is related to the inertial mode with $m_c = 2$ and $l = 5$. For larger values of $Pr > O(0.1)$, the inertial convection changes to the wall-localized convection for which the present analysis is no longer applicable. This will be discussed further in § 4.3.

Several typical critical parameters for inertial convection, calculated from both the asymptotic expressions and full numerics, are shown in table 5 for the case $\Gamma = 1$ and in table 6 for $\Gamma = 2$. Two asymptotic solutions in a cylinder with $\Gamma = 1$ for $Pr = 0.01$ and $Pr = 0.1$ are depicted in figure 7, both showing a multi-radial-layer structure as the azimuthal wavenumber increases from $m_c = 1$ at $Pr = 0.01$ to $m_c = 2$ at $Pr = 0.1$. A particularly interesting case, which is shown in figure 8 for $\Gamma = 2$, is the reversed direction of the wavenumber change. The critical wavenumber m_c decreases with

Pr	l	m_c	$(R_c, \sigma_c)_{asymptotic}$	$(R_c, \sigma_c)_{numerical}$
0	1	1	(0.340, 0.779)	(0.358, 0.779)
0.0025	1	3	(1.238, 0.485)	(1.243, 0.485)
0.005	1	4	(2.249, 0.405)	(2.240, 0.405)
0.01	3	1	(4.262, 0.325)	(4.298, 0.326)
0.025	3	2	(10.96, 0.270)	(10.71, 0.271)
0.05	4	2	(23.28, 0.205)	(22.84, 0.206)
0.1	5	1	(52.82, 0.157)	(51.08, 0.159)

TABLE 5. Several critical parameters at the onset of convection for different Prandtl numbers for $E = 10^{-4}$ and $\Gamma = 1$. Both the fully numerical and asymptotic solutions are shown. The sidewall of the cylinder is rigid and insulating.

Pr	l	m_c	$(R_c, \sigma_c)_{asymptotic}$	$(R_c, \sigma_c)_{numerical}$
0	2	1	(0.279, 0.747)	(0.281, 0.747)
0.0025	2	4	(0.914, 0.525)	(0.915, 0.525)
0.005	4	6	(1.712, 0.436)	(1.705, 0.436)
0.01	6	3	(3.418, 0.377)	(3.390, 0.377)
0.025	7	3	(9.195, 0.271)	(9.111, 0.271)
0.05	10	2	(20.82, 0.219)	(20.40, 0.219)
0.1	13	2	(49.06, 0.168)	(47.24, 0.169)

TABLE 6. Several critical parameters at the onset of convection for different Prandtl numbers for $E = 10^{-4}$ and $\Gamma = 2$. Both the fully numerical and asymptotic solutions are shown. The sidewall of the cylinder is rigid and insulating.

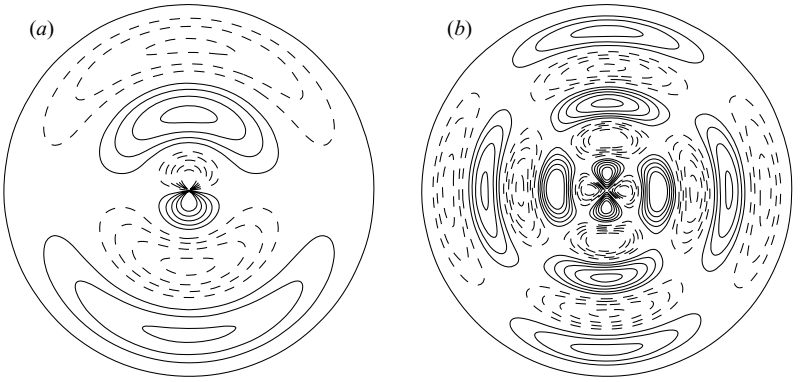

FIGURE 7. Contours of u_ϕ for two asymptotic solutions in the $z = 0.25$ plane for a cylinder with $\Gamma = 1$ at $E = 10^{-4}$: (*a*) $Pr = 0.01$ with critical parameters $m_c = 1$, $R_c = 4.26$, $\sigma_c = 0.325$ and (*b*) $Pr = 0.1$ with $m_c = 2$, $R_c = 52.82$, $\sigma_c = 0.157$. The sidewall of the cylinder is rigid and insulating.

increasing Pr: from $m_c = 6$ at $Pr = 0.005$ to $m_c = 3$ at $Pr = 0.025$ to $m_c = 2$ at $Pr = 0.1$. At the same time, the radial structure of the convection changes from three radial layers at $Pr = 0.005$ with $m_c = 6$ to six radial layers at $Pr = 0.01$ with $m_c = 3$ to ten radial layers at $Pr = 0.01$ with $m_c = 2$. Though the patterns of convection appear to be quite complex, it is remarkable that they are represented by relatively simple analytical functions given by (4.27)–(4.29).

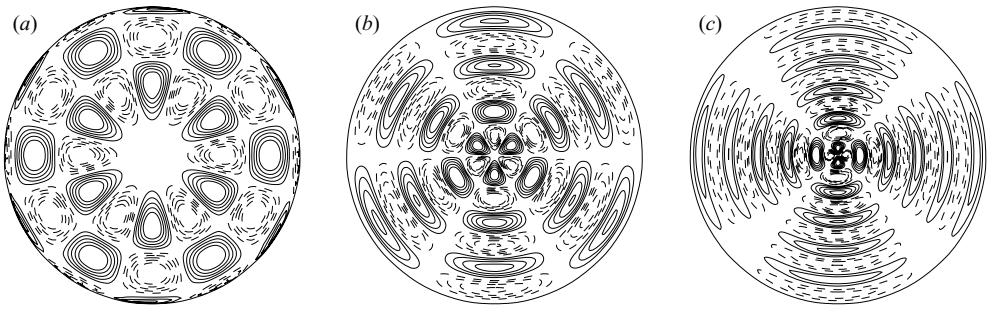

FIGURE 8. Contours of u_ϕ of three asymptotic solutions in the $z=0.25$ plane for a cylinder with $\Gamma=2$ at $E=10^{-4}$: (*a*) $Pr=0.005$ with $m_c=6$, $R_c=1.712$, $\sigma_c=0.436$, (*b*) $Pr=0.025$ with $m_c=3$, $R_c=9.19$, $\sigma_c=0.271$ and (*c*) $Pr=0.1$ with $m_c=2$, $R_c=49.06$, $\sigma_c=0.168$. The sidewall of the cylinder is rigid and insulating.

E	l	m_c	$(R_c, \sigma_c)_{asymptotic}$	$(R_c, \sigma_c)_{numerical}$
10^{-2}	1	1	(12.85, 0.751)	(14.04, 0.750)
10^{-3}	1	2	(3.505, 0.585)	(3.639, 0.586)
5×10^{-4}	1	3	(3.540, 0.474)	(3.654, 0.475)
10^{-4}	3	1	(4.262, 0.325)	(4.298, 0.326)
5×10^{-5}	3	2	(4.765, 0.277)	(4.744, 0.277)
10^{-5}	6	1	(6.536, 0.166)	(6.530, 0.166)
5×10^{-6}	7	1	(7.719, 0.142)	(7.667, 0.142)

TABLE 7. Several critical parameters at the onset of convection for different Ekman numbers for $Pr=0.01$ and $\Gamma=1$. Both the fully numerical and asymptotic solutions are shown. The sidewall of the cylinder is rigid and insulating.

We have so far concentrated on the case with the Ekman number $E=10^{-4}$. It is of considerable interest to look at how the asymptotic solution and fully numerical solution are dependent upon the Ekman number E. Several critical parameters for inertial convection, calculated from both the asymptotic expressions and full numerics, are shown in table 7 for various Ekman numbers with $\Gamma=1$. It is found that, as expected, the agreement between the asymptotic and fully numerical solutions is satisfactory only when the Ekman number is sufficiently small, $E\leqslant10^{-3}$. In contrast to convection in rotating spheres, the critical wavenumber m_c can decrease with decreasing E: from $m_c=3$ at $E=5\times10^{-4}$ to $m_c=1$ at $E=5\times10^{-6}$ to $m_c=1$. The change in the azimuthal wavenumber signifies the change in the radial structure of convection from the single radial layer to multiple layers. Displayed in figure 9 is the asymptotic solution in a cylinder with $\Gamma=1$ for $Pr=0.01$ and $E=5\times10^{-6}$, showing a seven-radial-layer structure with the azimuthal wavenumber $m_c=1$.

4.3. *The Pr-dependence: inertial vs. wall-localized modes*

Two conditions must be satisfied for the validity of asymptotic expansions like (4.16): the Ekman number E must be sufficiently small, $E\ll1$, and the modification of the inertial-wave frequency by convection must be also sufficiently small, i.e. $|\sigma_1/\sigma_0|\ll1$. The second condition implies that Pr must be sufficiently small compared to unity. For a given small E, it is difficult to identify the precise value of Pr, $\widehat{Pr}$, such that the asymptotic solution is mathematically valid for $0\leqslant Pr\leqslant\widehat{Pr}$. This is mainly

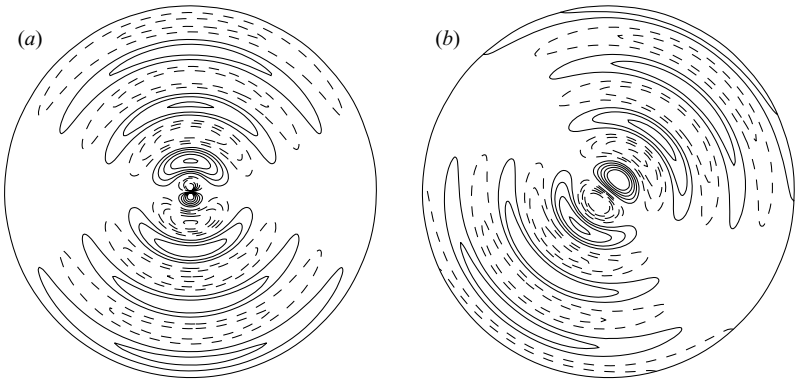

FIGURE 9. Contours of (*a*) u_ϕ and (*b*) Θ for the asymptotic solution in the $z=0.25$ plane for a cylinder with $\Gamma=1$ at $E=5\times10^{-6}$ and $Pr=0.01$. The sidewall of the cylinder is rigid and insulating.

caused by the fact that a simple solution for (2.5) cannot be obtained and, hence, the dependence between E and Pr is implicit.

The question of the mathematically valid domain for Pr is, however, physically unimportant. This is because there exist only two different types of convection in a rapidly ($E\ll1$) rotating cylinder with $\Gamma=O(1)$: inertial convection preferred for $0\leqslant Pr\leqslant Pr^*$ and wall-localized convection preferred for $Pr^*\leqslant Pr<\infty$, where Pr^* denotes the values of Pr at which the switch from the inertial to wall-localized mode occurs. Our analysis suggests that $Pr^*<\widehat{Pr}$, i.e. the asymptotic solution may be still mathematically valid in the sense that it gives a satisfactory approximation to equations (2.3)–(2.5) but is no longer physically relevant.

Let us illustrate this by looking at an example in a rotating cylinder with the no-slip and insulating sidewall for $E=10^{-4}$ and $\Gamma=1$. In this case, inertial convection described by the present asymptotic solution is preferred in the range $0\leqslant Pr<0.115$ while wall-localized convection becomes preferred for $0.115<Pr<\infty$. The switch-over from the inertial to wall-localized convection takes place at $Pr^*\approx0.115$. Figure 10 shows two convection solutions for $Pr=0.11$ and $Pr=0.12$ in the vicinity of the crossover. While the asymptotic solution (4.30) and (4.31) gives rise to $R_0=65, \sigma=0.14, m=1, l=6$ at $Pr=0.12$ (which exceeds Pr^*) the fully numerical solution yields $R_0=64, \sigma=0.14, m=1$ for this value of Pr. This means that the asymptotic solution for inertial convection still represents a reasonably accurate approximation. But it is the wall-localized convection characterized by a smaller Rayleigh number at $R_0=60$ that is physically realizable. Since $Pr^*<\widehat{Pr}$, the precise size of $\widehat{Pr}$ is of less interest and of secondary importance.

Evidently, the crossover value Pr^* cannot be determined by the current asymptotic theory, such as (4.30), alone. It can only be determined by comparing (4.30) to the corresponding expression for wall-localized convection (Herrmann & Busse 1993; Liao, Zhang & Chang 2006),

$$(R_c)_{inertial}(Pr^*, E)=(R_c)_{wall}(Pr^*, E), \tag{4.32}$$

which can in principle, be solved for the value of Pr^* at a given small E, providing the physically valid domain of inertial convection for Pr: $0\leqslant Pr\leqslant Pr^*$. In the case of a rotating cylinder with the no-slip and insulating sidewall for $E=10^{-4}$ and $\Gamma=1$, this comparison yields $Pr^*\approx0.115$.

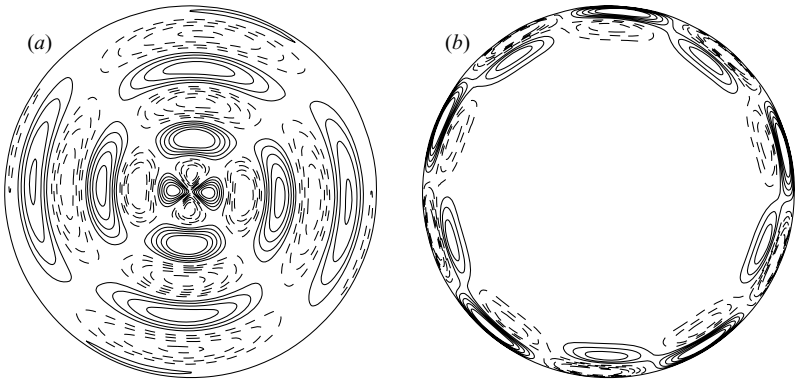

FIGURE 10. Contours of the azimuthal flow u_ϕ for two convection solutions (the most unstable modes) in the $z=0.25$ plane for a cylinder with $\Gamma=1$ at $E=10^{-4}$: (*a*) $Pr=0.11$ with $m_c=2$, $R_c=56.76$, $\sigma_c=0.157$ (inertial convection) and (*b*) $Pr=0.12$ with $m_c=5$, $R_c=60.49$, $\sigma_c=0.0183$ (wall-localized convection). The sidewall of the cylinder is rigid and insulating. The switch from the inertial to wall-localized mode occurs at $Pr\approx 0.115$.

5. Summary and remarks

This paper presents the first asymptotic theory for inertial convection in a rotating fluid cylinder. We have investigated, both numerically and analytically, inertial convection in a rotating cylinder heated uniformly from below. In the asymptotic analysis, the primary assumption is that the convective flow at leading order can be represented by one or several inertial wave modes. Buoyancy forces do not change the flow at the leading order but appear at next order to drive the inertial modes against the effects of viscous damping. In particular, we show that agreement between the asymptotic and numerical solutions is satisfactory in all the cases for moderately small $E=10^{-4}$. It is shown that the extremely complicated and seemly incomprehensible behaviour of convection in a rotating cylinder (see, for example, Goldstein *et al.* 1993, 1994) can be readily understood in the framework of small perturbations from solutions of the partial differential equation describing inertial waves.

In rapidly rotating cylinders, the dynamics of convection appears to be quite clear: convection is either of the inertial-wave type or of the wall-localized type. While inertial convection is preferred for small Prandtl numbers (weak effects of viscosity), wall-attached convection is preferred for large Prandtl numbers (strong effects of viscosity). The deeper reason for this behaviour is the effect of rapid rotation that constrains convection and strongly stabilizes the state of pure conduction. Wall-attached convection, which is largely independent of the cylindrical geometry, is preferred when the constraint is broken by viscous forces in association with small-scale convective flows. Inertial convection, which is critically influenced by the cylindrical geometry, offers an alternative at low Prandtl numbers when the rotational constraint on steady or quasi-steady forms of convection becomes too strong.

It is worth noting that we did not present our results in terms of the usual (Pr, m_c) or (Pr, ω_c) dependence, as frequently used for problems of convection in other geometries. Instead, the main results on inertial convection are primarily presented in tables. This style of our presentation reflects the nature of inertial convection. In general, there are no smooth connections between different convection modes. This is because the convection system selects its preferred pattern from a large manifold of all the inertial wave modes. In other words, a key feature in the present problem is

that the minimization must be done over a two-dimensional manifold of inertial wave modes through the evaluation of analytical expressions such as (4.12). This typically leads to a non-smooth dependence of properties like radial structure and azimuthal wavenumber of the preferred form of convection on the external parameters.

This work started in a 2004 summer workshop at the Newton Institute of Cambridge University. K.Z. would like to acknowledge helpful discussions with Professor E. Knobloch and is supported by UK PPARC, NERC and Leverhulme grants. X.L. is supported by NSFC grants 10633030. The numerical computation is supported by Shanghai Supercomputer Center.

Appendix

The zeroth order of the perturbation problem, resulting from the substitution of expansion (4.1) into equations (2.3)–(2.4), is given by

$$\mathrm{i}2\sigma_0\boldsymbol{u}_0 + 2\hat{\boldsymbol{z}}\times\boldsymbol{u}_0 + \nabla p_0 = 0, \tag{A 1}$$

$$\nabla\cdot\boldsymbol{u}_0 = 0, \tag{A 2}$$

where $(\boldsymbol{u}_0, p_0)$ denotes the solutions of the inviscid inertial wave obtained at $E=0$ and σ_0 is the half-frequency of the wave. For completeness, we shall discuss briefly the basic properties of the inertial wave in a rotating cylinder.

As a consequence of reducing the second-order differential equation (2.3) to the first-order equation (A 1), the existence of viscous boundary layers on the walls is not permitted. The velocity boundary condition is then relaxed to the condition of vanishing normal flow,

$$\hat{\boldsymbol{n}}\cdot\boldsymbol{u}_0 = 0, \tag{A 3}$$

at the bounding surface of the cylinder, where $\hat{\boldsymbol{n}}$ denotes the unit normal. It is the condition $\hat{\boldsymbol{s}}\cdot\boldsymbol{u}_0=0$ at the sidewall, however, that determines the eigenvalue, σ_0, of the problem (see, for example, Greenspan 1968). Solutions to (A 1)–(A 2) can be cast in the form

$$\left.\begin{aligned}\boldsymbol{u}_0 &= \boldsymbol{u}_0(s,z)\mathrm{e}^{\mathrm{i}(m\phi+2\sigma_0 t)},\\ p_0 &= p_0(s,z)\mathrm{e}^{\mathrm{i}(m\phi+2\sigma_0 t)},\end{aligned}\right\} \tag{A 4}$$

where m is the azimuthal wavenumber which is assumed to be positive. After simple mathematical manipulation, we can conveniently express the velocity components in terms of the pressure p_0:

$$\hat{\boldsymbol{s}}\cdot\boldsymbol{u}_0 = -\frac{\mathrm{i}}{2\left(1-\sigma_0^2\right)}\left(\sigma_0\frac{\partial p_0}{\partial s}+\frac{mp_0}{s}\right), \tag{A 5}$$

$$\hat{\boldsymbol{\phi}}\cdot\boldsymbol{u}_0 = \frac{1}{2\left(1-\sigma_0^2\right)}\left(\frac{\partial p_0}{\partial s}+\frac{m\sigma_0 p_0}{s}\right), \tag{A 6}$$

$$\hat{\boldsymbol{z}}\cdot\boldsymbol{u}_0 = \frac{\mathrm{i}}{2\sigma_0}\frac{\partial p_0}{\partial z}. \tag{A 7}$$

The elimination of the velocity $\boldsymbol{u}_0$ from (A 1)–(A 2) results in a single equation for the pressure:

$$\left(\frac{1}{s}\frac{\partial}{\partial s}+\frac{\partial^2}{\partial s^2}-\frac{m^2}{s^2}\right)p_0 - \left(\frac{1-\sigma_0^2}{\sigma_0^2}\right)\frac{\partial^2 p_0}{\partial z^2} = 0, \tag{A 8}$$

which is usually referred to as the Poincaré equation, a hyperbolic partial differential equation when $0 < |\sigma_0| < 1$. The inviscid boundary condition in terms of the pressure becomes

$$\frac{\partial p_0}{\partial z} = 0 \quad \text{at} \quad z = 0, 1 \tag{A 9}$$

and

$$\sigma_0 \frac{\partial p_0}{\partial s} + \frac{m}{s} \frac{\partial p_0}{\partial s} = 0 \quad \text{at} \quad s = \Gamma. \tag{A 10}$$

The Poincaré equation subject to the boundary condition (A 9)–(A 10) forms an eigenvalue problem with a special property that the eigenvalue appears in both the boundary condition and the governing equation. Solutions of separable variables for the Poincaré equation satisfying the condition (A 9) can be written in the form

$$p_0(s, z) = J_m\left(\frac{\xi s}{\Gamma}\right) \cos(n\pi z), \tag{A 11}$$

where $J_m(x)$ denotes the standard Bessel function and ξ is a solution of the transcendental equation

$$\xi \frac{\mathrm{d}J_m(\xi)}{\mathrm{d}\xi} + \frac{m\sigma_0}{|\sigma_0|}\left[1 + \left(\frac{\xi}{\Gamma n\pi}\right)^2\right]^{1/2} J_m(\xi) = 0. \tag{A 12}$$

The substitution of (A 11) into (A 5)–(A 7) yields the expressions of $\boldsymbol{u}_0$ for the inertial waves in a rotating cylinder:

$$\hat{\boldsymbol{s}} \cdot \boldsymbol{u}_0 = \frac{-\mathrm{i}}{2\left(1 - \sigma_0^2\right)}\left[\frac{\sigma_0 \xi}{\Gamma} J_{m-1}\left(\frac{\xi s}{\Gamma}\right) + \frac{m(1 - \sigma_0)}{s} J_m\left(\frac{\xi s}{\Gamma}\right)\right] \cos n\pi z, \tag{A 13}$$

$$\hat{\boldsymbol{\phi}} \cdot \boldsymbol{u}_0 = \frac{1}{2\left(1 - \sigma_0^2\right)}\left[\frac{\xi}{\Gamma} J_{m-1}\left(\frac{\xi s}{\Gamma}\right) - \frac{m(1 - \sigma_0)}{s} J_m\left(\frac{\xi s}{\Gamma}\right)\right] \cos n\pi z, \tag{A 14}$$

$$\hat{\boldsymbol{z}} \cdot \boldsymbol{u}_0 = \frac{-\mathrm{i}n\pi}{2\sigma_0}\left[J_m\left(\frac{\xi s}{\Gamma}\right)\right] \sin n\pi z. \tag{A 15}$$

In the context of inertial convection, only the inertial modes of the simplest z-structure with $n = 1$ are relevant to the most unstable mode of convective instabilities.

An inertial wave mode in a rotating cylinder can be described by a set of the triple numbers (m, n, σ_0): the wavenumber m always indicates the azimuthal scale of an inertial wave, n is related to the vertical structure and the size of σ_0 is indicative of not only how fast the wave propagates, but also of its radial structure. It is worth mentioning two important properties of the inertial wave solution: $|\sigma_0| < 1$ for all the inertial oscillation modes, and the orthogonal relationship

$$\int_0^1 \int_0^{2\pi} \int_0^{\Gamma} \boldsymbol{u}_{0j}(\sigma_{0j}) \cdot \boldsymbol{u}_{0k}^*(\sigma_{0k})\, s\mathrm{d}s\, \mathrm{d}\phi\, \mathrm{d}z = 0 \quad \text{if} \quad \sigma_{0j} \neq \sigma_{0k},$$

where $\boldsymbol{u}_{0k}^*$ denotes the complex conjugate of $\boldsymbol{u}_{0k}$, which will be used in our asymptotic analysis.

For a given wavenumber m, we can arrange all the inertial wave modes in the order of the largest positive, the second largest positive and so on. Negative half-frequencies can be arranged in the same way based on their absolute sizes. Several examples of the largest positive half-frequencies for the wavenumbers $m = 1, 2$ and $m = 3$ are given in table 8. To illustrate the radial structure of an inertial mode, we may attach an integer number l to each inertial mode according to the size of its half-frequency σ_0.

l	$\sigma_0(m=1)$	$\sigma_0(m=2)$	$\sigma_0(m=3)$
1	0.7808	0.6076	0.4921
2	0.4825	0.3914	0.3316
3	0.3338	0.2843	0.2495
4	0.2527	0.2224	0.1999
5	0.2026	0.1824	0.1666
6	0.1689	0.1544	0.1429

TABLE 8. Several largest positive σ_0 for three azimuthal wavenumbers with $n=1$ and $\Gamma=1$. The integer number $(l-1)$ corresponds to the number of zeros of $\hat{\boldsymbol{s}}_0 \cdot \boldsymbol{u}_0 = 0$ in $0 < s < \Gamma$.

For example, the $m=1$ inertial mode with the largest positive $\sigma_0 = 0.7808$ is labelled by an integer $l=1$ for which the radial component of the velocity $\hat{\boldsymbol{s}}_0 \cdot \boldsymbol{u}_0$ has no zero for $0 < s < \Gamma$. For the second inertial mode ($l=2$) with $\sigma_0 = 0.4825$ there is one zero for $0 < s < \Gamma$. In general, the lth inertial mode has $(l-1)$ zeros for $0 < s < \Gamma$. Furthermore it should be emphasized that $\boldsymbol{u}_0$ satisfies neither the stress-free nor the no-slip condition on the sidewall.

REFERENCES

BUSSE, F. H. & SIMITEV, R. 2004 Inertial convection in rotating fluid spheres. *J. Fluid Mech.* **498**, 23–30.

DAVIES-JONES, R. P. & GILMAN, P. A. 1971 Convection in a rotating annulus uniformly heated from below. *J. Fluid Mech.* **46**, 65–81.

HERRMANN, J. & BUSSE, F. H. 1993 Asymptotic theory of wall-localized convection in a rotating fluid layer. *J. Fluid Mech.* **255**, 183–194.

GOLDSTEIN, H. F., KNOBLOCH, E., MERCADER, I. & NET, M. 1993 Convection in a rotating cylinder. Part 1. Linear theory for moderate Prandtl numbers. *J. Fluid Mech.* **248**, 583–604.

GOLDSTEIN, H. F., KNOBLOCH, E., MERCADER, I. & NET, M. 1994 Convection in a rotating cylinder. Part 2. Linear theory for small Prandtl numbers. *J. Fluid Mech.* **248**, 583–604.

GREENSPAN, H. P. 1968 *The Theory of Rotating Fluids*. Cambridge University Press.

KERSWELL, R. R. & BARENGHI, C. F. 1995 On the viscous decay-rates of inertial waves in rotating circular cylinder. *J. Fluid Mech.* **285**, 215–247.

KUO, E. Y. & CROSS, M. C. 1993 Travelling-wave wall states in rotating Rayleigh-Benard convection. *Phys. Rev.* E **47**, 2245–2248.

LIAO, X., ZHANG, K. & CHANG, Y. 2005 Convection in rotating annular channels heated from below. Part 1. Linear stability and weakly nonlinear mean flows. *Geophys. Astrophys. Fluid Dyn.* **99**, 445–465.

LIAO, X., ZHANG, K. & CHANG, Y. 2006 On boundary-layer convection in a rotating fluid layer. *J. Fluid Mech.* **549**, 375–384.

LIU, Y. & ECKE, R. E. 1999 Nonlinear traveling waves in rotating Rayleigh-Bénard convection: Stability boundaries and phase diffusion. *Phys. Rev.* E **59**, 4091–4105

MARQUÉS, F. 1990 On boundary conditions for velocity potentials in confined flows: Application to Couette flow. *Phys. Fluids* A **2**, 729–737

PLAUT, E. 2003 Nonlinear dynamics of travelling Rayleigh-Bénard convection: effects of the boundary conditions and of the topology. *Phys. Rev.* E **67**, 046303

ZHANG, K. 1994 On coupling between the Poincaré equation and the heat equation. *J. Fluid Mech.* **268**, 211–229

ZHANG, K., EARNSHAW, P., LIAO, X. & BUSSE, F. H. 2001 On inertial waves in a rotating fluid sphere. *J. Fluid Mech.* **437**, 103–119.

ZHANG, K. & LIAO, X. 2004 A new asymptotic method for the analysis of convection in a rotating sphere. *J. Fluid Mech.* **518**, 319–346.

ZHONG, F., ECKE, R. E. & STEINBERG, V. 1991 Asymmetric modes and the transition to vortex structure in rotating Rayleigh-Benard convection. *Phys. Rev. Lett.* **67**, 2473–2476.